ANALYTICAL MODEL FOR NON-UNIFORM CORROSION-INDUCED CONCRETE CRACKING

Shangtong Yang[1], Kefei Li[2] and Chun-Qing Li[3*]

[1] Department of Civil and Environmental Engineering, University of Strathclyde, Glasgow, G1 1XJ, United Kingdom.

[2] Department of Civil Engineering, Tsinghua University, Beijing, 100084, China.

[3] School of Civil, Environmental and Chemical Engineering, RMIT University, GPO Box 2476, Melbourne 3001, Australia.

ABSTRACT

Corrosion-induced concrete cracking is one of the major deterioration mechanisms for reinforced concrete structures. Evidently, the corrosion process is not uniform along the circumference of the reinforcement. To model the stress distribution in concrete and determine the initiation of concrete cracking, a realistic non-uniform corrosion model needs to be developed. In this paper, a time-dependent corrosion model, producing non-uniform expansion to concrete, is first established. The stresses in concrete are then formulated through the employment of complex functions. The time to initiation of concrete cracking is determined and related to a number of material, geometric and corrosion parameters. The derived analytical model is verified by comparing the results with those from experimental tests in literature. It can be concluded that this model is one of very few analytical models that can determine the stresses in concrete caused by non-uniform corrosion of reinforcement in concrete.

KEYWORDS: Durability-related properties; Fracture & fracture mechanics; Cracks & cracking.

* Corresponding author. Tel: +61 3 9925 2181. Email: chunqing.li@rmit.edu.au.

INTRODUCTION

Corrosion of reinforcement is a significant problem affecting the durability of reinforced concrete (RC) structures. Practical experience and experimental observations (Andrade et al., 1993, Li, 2003, Otsuki et al., 2000) suggest that corrosion affected RC structures deteriorate faster in terms of serviceability (e.g., cracking or deflection) than safety (e.g., strength). Consequently, corrosion can lead to premature deterioration of RC structures, causing concrete cracking, delaminating and de-bonding. For example, only 4% to 5% degree of corrosion (in terms of steel mass loss) can cause serviceability failure of RC structures as defined by corrosion-induced crack width (El Maaddawy et al., 2005). Moreover, the maintenance and repair costs for corrosion induced deterioration in RC bridges in the United States have been reported more than $5 billion per year (Koch et al., 2002).

Realising the significance of the problem, considerable research has been conducted during the last few decades. Early work mainly focused on uniform corrosion along the circumference of the reinforcing rebar in concrete (Liu and Weyers, 1998). This was probably because most experiments on producing corrosion in reinforced concrete employed impressed current technique; such an accelerated corrosion method controls the corrosion rate, hence the degree of corrosion, by adjusting the current and/or the time of interval applied to the reinforcement. As such, the corrosion generated by the impressed current method is in a uniform manner along the rebar. Meanwhile, almost all of the analytical and numerical studies assume a uniform corrosion expansion exerting between the reinforcement and its surrounding concrete. Under the corrosion expansion, concrete has been often modelled as a thick-wall cylinder (Bazant, 1979, Pantazopoulou and Papoulia, 2001, Li et al., 2006). Liu and Weyers (1998) proposed an analytical solution for the time to surface cracking by presuming concrete linear elastic and the

uniform corrosion development. This analytical model has soon been improved by a number of researchers, e.g., (Pantazopoulou and Papoulia, 2001, Li et al., 2006, Bhargava et al., 2006), who considered concrete as a quasi-brittle material, i.e., the fracture property of concrete being included in the models. These models can well address the corrosion-induced cracking behaviour, covering time to cracking initiation, time to surface cracking, surface crack width, etc. However, the limitation is that only uniform boundary condition can be applied to the formulation of the stress and strain in concrete.

More recently, modelling of corrosion-induced cracking of concrete has been focused on non-uniform corrosion progression at the interface between reinforcement and concrete. Due to the fact that chlorides, as well as moisture and oxygen, penetrates to the depth of the reinforcement at different rates on different sides of the concrete, it is very rare to have a uniform and general corrosion on the reinforcement. It has been reported (González et al., 1995) that the pitting caused localized deterioration is equivalent to about four to eight times that of the reinforcement under overall corrosion. To study the non-uniform corrosion caused structural deterioration, numerical approach, mainly finite element method (FEM), has played a dominating role (Jang and Oh, 2010, Pan and Lu, 2012, Zhao et al., 2011, Du et al., 2014). Jang and Oh (2010) considered a few of non-uniform distributions of corrosion products and simulated the stress states in concrete accordingly. Pan and Lu (2012) modelled the non-uniform corrosion caused crack propagation in concrete with FEM and the concrete as a heterogeneous material. Du et al. (2014) employed damage plasticity model to simulate the concrete cracking under non-uniform corrosion induced expansion. A number of parameters were investigated on their effects to the surface cracking. Zhao et al. (2011) proposed a Gaussian distribution for the non-uniform corrosion caused displacement and simulated the cracking behaviour of concrete by smeared crack model. Literature review suggests (1) the

77 distribution of the non-uniform corrosion caused expansion has seldom been based on
78 experimental test results but more on assumptions and; (2) no model has been developed in
79 relating concrete cracking to some basic parameters for the non-uniform corrosion, e.g.,
80 corrosion rate. As pointed out in (Zhao et al., 2011), this is probably because there is an absence
81 of reliable data which can characterize the actual non-uniform formation and expansion of the
82 corrosion products.
83
84 Yuan and Ji (2009) conducted the accelerated corrosion tests on reinforced concrete samples in
85 an artificial environmental chamber and obtained a non-uniform corrosion distribution along
86 the interface between reinforcement and concrete. In their findings, only a half of the
87 reinforcement, facing concrete cover, was corroded and the corrosion caused expansion was in
88 a semi-elliptical shape. Amongst limited experimental data, the non-uniform distribution
89 derived from Yuan and Ji (2009) can provide the reasonable inputs for modelling the
90 non-uniform corrosion caused concrete cracking. Moreover, although numerical approaches
91 are more powerful in terms of solving a wider range of problems, analytical solutions are more
92 accurate and convenient for the practical application. It would be, therefore, ideal to have an
93 analytical model on non-uniform corrosion induced cracking of concrete. In the analytical
94 model, some key material and corrosion parameters, e.g., corrosion rate, can be related to the
95 structural behaviour, e.g., time to cracking. However, the non-uniform stress distribution, along
96 the hoop direction of the concrete cylinder, requires complex functions to be used in the
97 analytical formulation. In this case, concrete can only be treated as an elastic material, with
98 cracking initiation being modelled. The initiation of cracking in concrete marks the start of the
99 structural deterioration of reinforced concrete structures. After that the structure usually
100 degrades faster and reaches to limit states quickly.

This paper attempts to develop an analytical model for non-uniform corrosion induced concrete cracking. A time-dependent non-uniform corrosion model is first derived, based on realistic experimental results from literature. A cracking model is then formulated by using the complex functions to account for the non-uniform stress distribution on concrete. A number of material, geometric and corrosion parameters are considered in the analytical model. The initiation of the concrete cracking is determined as a function of its service time.

RESEARCH SIGNIFICANCE

Although considerable research has been conducted on modelling corrosion-induced concrete cracking problems, very few models have been proposed based on non-uniform corrosion of reinforcement in concrete. Amongst these available models for non-uniform corrosion, most employed numerical approaches while almost none on an analytical manner. However, it has become a widely accepted fact that the corrosion of reinforced concrete is normally not uniform. For accurate prediction of cracking caused by corrosion, it is necessary to consider non-uniform corrosion expansion in the formulation of stress and strain in the concrete solid. It is therefore imperative to derive a rational model for corrosion-induced concrete cracking to achieve the cost effectiveness in the asset management of reinforced concrete structures. To the best knowledge of the authors, this paper represents the first attempt in the analytical formulation of time-dependent non-uniform corrosion induced concrete cracking.

NON-UNIFORM CORROSION MODEL

Concrete with an embedded bar subjected to an internal pressure at the interface between the bar and concrete can be modelled as a thick-wall cylinder (Bazant, 1979, Pantazopoulou and Papoulia, 2001, Tepfers, 1979). This is schematically shown in Figure 1(a), where D is the

125 diameter of the bar; d_0 is the thickness of the annular layer of concrete pores at the interface
126 between the bar and concrete; and C is the concrete cover. Usually d_0 is constant once
127 concrete has hardened. The inner and outer radii of the cylinder are $a = D/2 + d_0$ and
128 $b = C + D/2 + d_0$.

129
130 The corrosion products (mainly ferrous and ferric hydroxides, *$Fe(OH)_2$ and $Fe(OH)_3$*) occupy a
131 few times more space than the original steel. The corrosion products first fill in the annular
132 pores in concrete around the reinforcing bar, with thickness d_0, but normally do not produce
133 stresses in concrete. As corrosion propagates in concrete, a band of corrosion products forms, as
134 shown in Figure 1(b). If the reinforcement corrosion is a uniform process along the
135 circumference of the reinforcing bar, the band becomes a circular ring which causes uniform
136 expansive pressure on the concrete cylinder (Li et al., 2006). However, this is usually not
137 realistic as discussed earlier. It has been found that (Yuan and Ji, 2009), the front of corrosion
138 products for the half of rebar facing concrete cover is in a semi-elliptical shape, while corrosion
139 of the opposite half of rebar is negligibly small and can be neglected.

140
141
142 The total amount of corrosion products $W_{rust}(t)$ can be assumed to distribute around the bar,
143 occupying three parts as shown in Figure 1(c): the semi-elliptical band of corroded steel with
144 maximum thickness d_{co-st}, the porous circular band d_0 and the semi-elliptical rust band with
145 maximum thickness d_m. It should be noted that the semi-major axis for the semi-ellipse of
146 corrosion front is $D/2 + d_0 + d_m$. $W_{rust}(t)$ can thus be expressed as follows:

147
148
$$W_{rust}(t) = W_s + W_0 + W_m \tag{1}$$
149

Where W_s is the amount of rust replacing the corroded steel, W_0 is the amount of rust filling the porous band d_0 and W_m is the amount of rust in the band d_m. W_s, W_0 and W_m can be derived respectively as follows:

$$W_s = \alpha_{rust} W_{rust} \frac{\rho_{rust}}{\rho_{st}} \tag{2}$$

$$W_0 = \frac{\pi \rho_{rust} (D + d_0) d_0}{2} \tag{3}$$

$$W_m = \rho_{rust} \left[\frac{\pi}{2} \left(\frac{D}{2} + d_0 \right) \left(\frac{D}{2} + d_0 + d_m \right) - \frac{\pi}{2} \left(\frac{D}{2} + d_0 \right)^2 \right] = \frac{\pi \rho_{rust}}{2} \left(\frac{D}{2} + d_0 \right) d_m \tag{4}$$

α_{rust} is the molecular weight of steel divided by the molecular weight of corrosion products. It varies from 0.523 to 0.622 according to different types of corrosion products (Liu and Weyers, 1998). ρ_{rust} is the density of corrosion products.

By substituting Equations (2-4) into Equations (1), it becomes:

$$\frac{2W_{rust}(t)}{\pi} \left(\frac{1}{\rho_{rust}} - \frac{\alpha_{rust}}{\rho_{st}} \right) = D d_0 + d_0^2 + \frac{D}{2} d_m + d_0 d_m \tag{5}$$

By neglecting the second order of small quantities, i.e., $d_0 d_m$ and d_0^2, d_m can be derived as follows:

$$d_m(t) = \frac{4W_{rust}}{\pi D} \left(\frac{1}{\rho_{rust}} - \frac{\alpha_{rust}}{\rho_{st}} \right) - 2d_0 \tag{6}$$

$d_m(t)$ in Equation (6) is the maximum corrosion-induced expansion along the interface to the concrete cylinder under which the stress will be initiated in the cylinder. $d_m(t)$ determines the

shape of the semi-ellipse which is the boundary condition of the concrete cylinder in deriving stresses and strains in concrete.

In Equation (6), $W_{rust}(t)$ is related to the corrosion rate of the steel rebar and can be expressed as (Liu and Weyers, 1998):

$$W_{rust}(t) = \sqrt{2\int_0^t 0.105(1/\alpha_{rust})\pi D i_{corr}(t)dt} \tag{7}$$

where i_{corr} is the corrosion current density in $\mu A/cm^2$, which is widely used as a measure of corrosion rate.

The units of the parameters in Equations (1-7) need to keep consistent. For the clarification and also the convenience of readers, the units are specified in Table 1.

To determine the displacement boundary condition of the concrete cylinder, the function of the semi-ellipse of the corrosion front needs to be derived. It is known that, in rectangular coordinate system, the function for an ellipse can be expressed as follows:

$$\frac{y^2}{A_L^2} + \frac{x^2}{A_S^2} = 1 \tag{8}$$

where A_L is the half length of major axis and A_S is the half length of the minor axis for an ellipse, as shown in Figure 2. The bottom half of the circular band d_0 is shaded for easier recognition of the three bands, e.g., d_{co-st}, d_0 and d_m. Based on the geometry in Figure 2, A_L and A_S can be obtained, i.e., $A_L = D/2 + d_0 + d_m$ and $A_S = D/2 + d_0$.

Transforming to a polar coordinate system, Equation (8) can be rewritten as follows,

$$r = \frac{A_L A_S}{\sqrt{A_S^2 \sin^2\theta + A_L^2 \cos^2\theta}} \tag{9}$$

Substituting A_L and A_S in the above equation,

$$r = \frac{(D + 2d_0 + 2d_m)(D + 2d_0)}{\sqrt{(2D + 4d_0)^2 + 16d_m(D + 2d_0 + d_m)\cos^2\theta}} \tag{10}$$

The displacement boundary condition of the concrete cylinder $\delta(\theta, t)$ can therefore be derived, with d_m substituted in Equation (6):

$$\delta(\theta,t) = \frac{\left[D + 2d_0 + \frac{8W_{rust}(t)}{\pi D}\left(\frac{1}{\rho_{rust}} - \frac{\alpha_{rust}}{\rho_{st}}\right) - 4d_0\right](D + 2d_0)}{\sqrt{(2D + 4d_0)^2 + 32\left[\frac{2W_{rust}(t)}{\pi D}\left(\frac{1}{\rho_{rust}} - \frac{\alpha_{rust}}{\rho_{st}}\right) - d_0\right]\left[D + 2d_0 + \frac{4W_{rust}(t)}{\pi D}\left(\frac{1}{\rho_{rust}} - \frac{\alpha_{rust}}{\rho_{st}}\right) - 2d_0\right]\cos^2\theta}} - \frac{D}{2} - d_0 \tag{11}$$

where $0 \le \theta \le \pi$.

CONCRETE CRACKING MODEL

As discussed, the concrete is modelled as a thick wall cylinder. In polar coordinate system, the stress components in plane stress/strain elastic body can be expressed in terms of two arbitrary complex functions $\gamma(z)$ and $\psi(z)$ (Sadd, 2005) as follows:

$$\sigma_r + \sigma_\theta = 2\left[\gamma'(z) + \overline{\gamma'(z)}\right] \tag{12}$$

$$\sigma_\theta - \sigma_r + 2i\tau_{r\theta} = 2\left[\bar{z}\gamma''(z) + \psi'(z)\right]e^{2i\theta} \tag{13}$$

where σ_r is the radial stress component, σ_θ is the hoop stress component and $\tau_{r\theta}$ is the shear stress component.

Solving the Equations (12) and (13) the individual stress components can be derived as follows,

$$\sigma_r = \mathrm{Re}\left[2\gamma'(z) - \bar{z}\gamma''(z)e^{2i\theta} - \psi'(z)e^{2i\theta}\right] \quad (14)$$

$$\sigma_\theta = \mathrm{Re}\left[2\gamma'(z) + \bar{z}\gamma''(z)e^{2i\theta} + \psi'(z)e^{2i\theta}\right] \quad (15)$$

$$\tau_{r\theta} = \mathrm{Im}\left[\bar{z}\gamma''(z)e^{2i\theta} + \psi'(z)e^{2i\theta}\right] \quad (16)$$

The solution to the complex functions $\gamma(z)$ and $\psi(z)$ relies on solving the boundary conditions of the hollow circular cylinder. There are two types of boundary conditions that can be formulated, i.e., stress boundary condition and displacement boundary condition. These conditions can be expressed as follows:

$$\gamma(z) + z\overline{\gamma'(z)} + \overline{\psi(z)} = iF(z) \quad \text{for stress boundary condition} \quad (17)$$

$$\kappa\gamma(z) - z\overline{\gamma'(z)} - \overline{\psi(z)} = 2G\delta(z) \quad \text{for displacement boundary condition} \quad (18)$$

where $F(z)$ is the resultant force exerting on a boundary, G is the shear modulus, δ is the displacement exerting on a boundary. $\kappa = 3 - 4\upsilon$ for plane strain problem and $\kappa = \frac{3-\upsilon}{1+\upsilon}$ for plane stress problem, while υ is the Poisson's ratio.

As discussed, the expansive mechanism is modelled as displacement boundary condition to the inner circle of the concrete cylinder. The inner boundary condition can be expressed as follows,

$$\kappa\gamma(z_1) - z_1\overline{\gamma'(z_1)} - \overline{\psi(z_1)} = 2G\delta(z_1, t), \qquad z_1 = ae^{i\theta} \quad (19)$$

The outer boundary is the surface of the concrete cover. Therefore, the stress condition can be formulated as follows,

$$\gamma(z_2) + z_2\overline{\gamma'(z_2)} + \overline{\psi(z_2)} = iF(z_2) = 0, \qquad z_2 = be^{i\theta} \quad (20)$$

According to Laurent's Theorem, each complex potential can be expressed as a power series, reducing the stress and/or displacement boundary problems to sets of simultaneous linear equations in the coefficients of the two power series (MuSkhelishvili, 1953).

$$\gamma(z)=\sum_{-\infty}^{+\infty}\alpha_n z^n \tag{21}$$

$$\psi(z)=\sum_{-\infty}^{+\infty}\beta_n z^n \tag{22}$$

where $a \le |z| \le b$. Substituting Equations (21) and (22) into the stress boundary condition, i.e., Equation (20), it becomes

$$\sum_{-\infty}^{+\infty}\alpha_n {z_2}^n + z_2\sum_{-\infty}^{+\infty} n\overline{\alpha_n}\,\overline{z_2}^{n-1} + \sum_{-\infty}^{+\infty}\overline{\beta_n}\,\overline{z_2}^{n} = 0 \ , \qquad \text{for } z_2 = be^{i\theta} \tag{23}$$

For the sake of simplifying Equation (23), both sides of the equation are multiplied by $e^{-im\theta}$ ($m = 0$ or integer), followed by integration with respect to θ from 0 to 2π. The boundary condition (Equation 23) then becomes:

$$\sum_{-\infty}^{+\infty}\alpha_n b^n \int_0^{2\pi} e^{in\theta}e^{-im\theta}d\theta + be^{i\theta}\sum_{-\infty}^{+\infty} n\overline{\alpha_n} b^{n-1}\int_0^{2\pi} e^{-i(n-1)\theta}e^{-im\theta}d\theta + \sum_{-\infty}^{+\infty}\overline{\beta_n} b^n \int_0^{2\pi} e^{-in\theta}e^{-im\theta}d\theta = 0 \tag{24}$$

It can be mathematically proved that, $\int_0^{2\pi} e^{in\theta}d\theta = 0$ if n is an integer or 2π if $n = 0$. Therefore Equation (24) can be simplified as follows:

$$b^{2m}\alpha_m + (2-m)b^2\overline{\alpha}_{2-m} + \overline{\beta}_{-m} = 0 \tag{25}$$

Similarly, by substituting the power series, the inner displacement boundary condition, i.e., Equation (19), becomes,

$$\kappa\sum_{-\infty}^{+\infty}\alpha_n {z_1}^n - z_1\sum_{-\infty}^{+\infty} n\overline{\alpha_n}\,\overline{z_1}^{n-1} - \sum_{-\infty}^{+\infty}\overline{\beta_n}\,\overline{z_1}^{n} = 2G\delta(\theta,t), \qquad \text{for } z_1 = ae^{i\theta} \tag{26}$$

Substituting $z_1 = ae^{i\theta}$, multiplying $e^{-im\theta}$ and integrating with respect to θ from 0 to 2π, Equation (26) can be simplified as follows:

$$\kappa a^{2m}\alpha_m - (2-m)a^2\overline{\alpha}_{2-m} - \overline{\beta}_{-m} = \frac{a^m G}{\pi}\int_0^{2\pi}\delta(\theta,t)e^{-im\theta}d\theta \tag{27}$$

By combining Equation (25) and (27), α_m and β_m can be derived.

$$\alpha_m = \frac{(2-m)(a^2-b^2)a^{2-m}G\int_0^{2\pi}\overline{\delta}(\theta,t)e^{i(2-m)\theta}d\theta + \left[\kappa a^{2(2-m)} + b^{2(2-m)}\right]a^m G\int_0^{2\pi}\delta(\theta,t)e^{-im\theta}d\theta}{\pi\left\{(\kappa a^{2m}+b^{2m})\left[\kappa a^{2(2-m)}+b^{2(2-m)}\right] - m(2-m)(a^2-b^2)^2\right\}} \tag{28}$$

$$\beta_m = \frac{\pi\left[\kappa a^{-2(m+1)} + b^{-2(m+1)}\right]\overline{\alpha}_{-m} + a^{-(m+2)}G\int_0^{2\pi}\overline{\delta}(\theta,t)e^{-im\theta}d\theta}{\pi\left(a^{-2}+b^{-2}\right)} \tag{29}$$

To solve α_m and β_m with regards to the integrals in Equations (28) and (29), $\delta(\theta,t)$, i.e., Equation (11), needs to be expanded to Fourier series as follows (MuSkhelishvili, 1953):

$$\delta(\theta,t) = \sum_{k=-\infty}^{+\infty} A_k e^{ik\theta} \tag{30}$$

where $A_k = \frac{1}{2\pi}\int_0^{2\pi}\delta(\theta,t)e^{-ik\theta}d\theta$.

It is difficult to derive the explicit integrated form of series coefficients A_k; however, those coefficients can be determined by numerical integration once all the other parameters are evaluated.

Substituting Equations (30) into Equations (28) and (29),

277 $$\alpha_m = \frac{(2-m)(a^2-b^2)a^{2-m}G\sum_{-\infty}^{+\infty}A_k\int_0^{2\pi}e^{i(2-k-m)\theta}d\theta + \left[\kappa a^{2(2-m)}+b^{2(2-m)}\right]a^m G\sum_{-\infty}^{+\infty}A_k\int_0^{2\pi}e^{-i(k+m)\theta}d\theta}{\pi\left\{(\kappa a^{2m}+b^{2m})\left[\kappa a^{2(2-m)}+b^{2(2-m)}\right]-m(2-m)(a^2-b^2)^2\right\}}$$

278 (31)

279 $$\beta_m = \frac{\pi\left[\kappa a^{-2(m+1)}+b^{-2(m+1)}\right]\overline{\alpha}_{-m} + a^{-(m+2)}G\sum_{-\infty}^{+\infty}A_k\int_0^{2\pi}e^{-i(k+m)\theta}d\theta}{\pi\left(a^{-2}+b^{-2}\right)} \quad (32)$$

280 Since $\int_0^{2\pi}e^{in\theta}d\theta = 0$ if n is an integer or 2π if $n=0$, α_m and β_m can be determined.

281 $$\alpha_m = \frac{2(2-m)(a^2-b^2)a^{2-m}GA_{2-m} + 2\left[\kappa a^{2(2-m)}+b^{2(2-m)}\right]a^m GA_{-m}}{(\kappa a^{2m}+b^{2m})\left[\kappa a^{2(2-m)}+b^{2(2-m)}\right]-m(2-m)(a^2-b^2)^2} \quad (33)$$

282 $$\beta_m = \frac{\left[\kappa a^{-2(m+1)}+b^{-2(m+1)}\right]\overline{\alpha}_{-m} + 2a^{-(m+2)}GA_{-m}}{a^{-2}+b^{-2}} \quad (34)$$

283 where m is an integer or 0. The Fourier coefficients A_k can be numerically determined in
284 MatLab and therefore α_m and β_m are solved. By substituting α_m and β_m into Equations (21)
285 and (22), the stress components, i.e., σ_r, σ_θ and $\tau_{r\theta}$, can be calculated from Equations (14) –
286 (16).
287
288 **WORKED EXAMPLE**

289 To demonstrate the application of the derived model, a numerical example is undertaken on a
290 reinforced concrete beam originally investigated in (Li, 2003). The corrosion was achieved via
291 saltwater spray in a customer designed environmental chamber. The values of basic variables of
292 the structure and corrosion are shown in Table 2.
293

With these values of the basic variables, first of all, the corrosion caused expansion (displacement) can be obtained. $d_m(t)$ in Equation (6), defining the shape of the inner displacement boundary condition of the concrete cylinder, is illustrated as a function of service time (10 years), shown in Figure 3. Such a development of corrosion expansion is based on the assumption that the corrosion rate i_{corr} is time-dependent and equal to $0.3686ln(t)+1.1305$ μ A/cm^2 (Li, 2003). The inset in Figure 3 represents an enlarged picture showing the initial progression of the corrosion products. It can be seen that the maximum displacement $d_m(t)$ starts to increase from zero at around 0.2 year, which is then followed by gradual increase in the subsequent lifetime. Once $d_m(t)$ is obtained, the whole inner boundary condition of the concrete cylinder, represented by Equation (11), can be determined.

Under the non-uniform expansion caused by reinforcement corrosion, the stresses can be calculated from Equations (14) – (16). Figures 4 and 5 show the hoop and radial stresses, respectively, at the inner boundary of the concrete cylinder at 0.23 year. As illustrated in Figure 1 – c, the point of zero degree is located at the right middle of the inner boundary, with [0, $-\pi/2$] represents the top right quarter and [0, $\pi/2$] represents the bottom right quarter, of the concrete cylinder. The whole cylinder is symmetric against the y-axis, as shown in Figure 2. It can be seen that the hoop stress changes along the inner boundary, most of which is under tension. It has been found the highest hoop stress occurs at the location close to 15^o. This is the location where the crack is initiated. Although most of the concrete is in tension, a small part of the concrete cylinder, from 80^o to 90^o, is under mild compression in the hoop direction. It is worth to mention that the maximum displacement $d_m(t)$ of the elliptical shape of the boundary condition is added at the location of 90^o. The combined tension and compression distribution of hoop stress is quite different than previous findings by assuming uniform corrosion expansion

where the hoop stresses of the concrete are all in tension, e.g., in (Li and Yang, 2011). Under the non-uniform expansion, the point at 90^o location appears to have the largest radial and compressive stress. At the region around 15^o the radial stress is in tension. It is very interesting to find, under the non-uniform corrosion expansion, the 90^o location is in compression in both hoop and radial directions, whilst the 15^o location is in tension in both directions. It should be noted that the positive hoop stress in Figure 4 represents tensile stress while the positive radial stress in Figure 5 represents compressive stress.

VALIDATION OF THE DEVELOPED MODEL

The derived model is verified by comparing the time to cracking initiation of the model and the experimental results from literature. According to the literature searched, almost all the test data regarding the time to cracking initiation are based on uniform corrosion development by electric current method for accelerated corrosion. For the limited experimental research on non-uniform corrosion by utilizing artificial environmental chamber with salt spray function, no data on time to cracking initiation was provided. In light of comparing the derived model with the test results, a special case of uniform corrosion was solved based on the developed model. The stresses were then computed by the derived analytical equations and the time to cracking initiation was determined, according to given tensile strength of the concrete. The values for all inputs were made the same between the analytical model and the experiment. The corrosion rate i_{corr} is time-dependent in this model; but for the purpose of comparison, $i_{corr} = 100 \mu A / cm^2$ was used as was applied in the test (Mullard and Stewart, 2011). The comparison to the experimental results is shown in Table 3. The results from the analytical model and the experimental tests are in reasonable agreement. Further, it is interesting to find that all the modelled times to cracking initiation are larger than the experimental ones. This is

342 probably because the assumption of the ITZ in the model, i.e., it is totally stress-free when the
343 corrosion products are filling the band of ITZ. In fact, however, the filling of the corrosion
344 products in the porous ITZ can cause pressure. As a result, such an assumption of the ITZ will
345 underestimate the pressure induced by corrosion. The effect of the thickness d_0 of the ITZ will
346 be elaborated in the following section and illustrated in Figure 8.
347
348 **ANALYSIS AND DISCUSSION**

349 Corrosion rate, normally expressed as corrosion current density i_{corr}, has been considered one
350 of the key factors affecting the durability of reinforced concrete structures. A number of
351 researchers have been working on developing realistic models for the corrosion rate; in the
352 worked example, a time-dependent corrosion rate was employed. To investigate the effects of
353 the corrosion rate on the corrosion caused expansion, i.e., $d_m(t)$, 4 constants corrosion rates are
354 used, i.e., $i_{corr}=0.5\mu A/cm^2$, $i_{corr}=1.0\mu A/cm^2$, $i_{corr}=5\mu A/cm^2$ and $i_{corr}=10\mu A/cm^2$, as
355 presented in Figure 6(a). These corrosion rates are believed to have covered a wide range of
356 actual corrosion states of reinforced concrete structures. It can be seen that, as expected, the
357 increase of the corrosion rate will cause the increase of expansive displacement to the concrete.
358 The long-term effect is significant; for example, as the corrosion rate grows up to 10 times, the
359 10-year maximum displacement $d_m(t)$ could be increased to about 3.5 times. Such an increase
360 magnitude in the displacement boundary condition is crucial to the stress development in the
361 concrete cylinder. Nevertheless, the short-term effect is more sensitive, as shown in Figure
362 6(b). The corrosion rate $i_{corr}=10\mu A/cm^2$ causes immediate form and progression of the rust
363 band at 0.01 year, whilst the pushing over of the rust band to the concrete cylinder is delayed to
364 0.19 year for the corrosion rate $i_{corr}=0.5\mu A/cm^2$. Further, the initial slope of the development

365 of $d_m(t)$ is considerably steeper for higher corrosion rates. This means the initiation of cracking
366 might be very sensitive to the corrosion rate.
367
368 Figure 7 shows the development of $d_m(t)$ as the diameter of the reinforcing rebar changes.
369 When the diameter of the rebar increases from 12mm to 20mm, the time to the initial
370 progression of $d_m(t)$ is delayed slightly, i.e., 0.06 year. The long-term development of $d_m(t)$
371 against the service time is also reduced as the diameter of rebar increases. This proves that, for
372 the same corrosion rate, larger size of rebar favours the corrosion caused expansion and hence
373 delays the cracking initiation of the concrete.
374
375 Figure 8 demonstrates the effects of the ITZ thickness on the accumulation of the corrosion
376 products. Three reasonable values of thickness are selected for the calculation of $d_m(t)$. As
377 expected, the increase of the ITZ thickness can delay the occurrence of the expansive
378 displacement. This is mainly because in this paper the porous ITZ is assumed to fully
379 accommodate the corrosion products; as a result, the process of the accumulation of corrosion
380 products in ITZ, does not cause any stress or displacement. In Figure 8, it has been found that
381 the effect of ITZ thickness on the initial stage of $d_m(t)$ progression is quite considerable, with
382 the delay of roughly 83% from 0.18 year to 0.33 year for $d_0 = 12e-6m$ and $d_0 = 20e-6m$,
383 respectively. However, the long-term effects on $d_m(t)$ seems not very significant.
384
385 Figure 4 has shown the maximum tensile stress occurs at the location of around 15^0, as a result
386 of the non-uniform corrosion expansion modelled. It is therefore worth to plot the hoop stress

development history of this point. Figure 9 presents the hoop stress development as a function of service time for the point of 15°. The hoop stress for this point keeps constantly zero until 0.19 year which is followed by a very quick increase up to about 6MPa at 0.23 year. Most concrete will be cracked at such a level of tensile stress. The initial period of 0.19 year mainly represents the time for corrosion products propagating into the porous ITZ. Moreover, the initial 0.23 year represents for the initiation of cracking which marks the start of structural degradation.

Figure 10 shows the radial stress development for the point of 90° under the derived non-uniform corrosion model. This point is where the maximum displacement $d_m(t)$ is applied and the maximum compressive stress occurs. Although the main failure type of this problem is fracture which is caused by tension, Figure 10 could be useful as to indicating the extent of compression at the time of cracking initiation.

By knowing the tensile strength of concrete f_t, the time to cracking initiation can be obtained. This is based on the failure criterion of the tensile stress reaches the tensile strength of concrete. As specified in Table 2, f_t=5.725MPa is used in this study; hence the effect of corrosion rate on the time to initiation of cracking can be determined, as shown in Figure 11. Four corrosion rates are considered and fitted curve (R^2=1) was produced according to these four points. It can be seen that for minor corrosion extent, e.g., i_{corr} is between $0.5\mu A/cm^2$ and about $3.0\mu A/cm^2$, the time to cracking initiation is very sensitive to the corrosion rate; however, when i_{corr} is larger than $3.0\mu A/cm^2$, the change in time to initiation of cracking is very small.

CONCLUSIONS

In the paper, the stresses in concrete, subjected to non-uniform corrosion of the reinforcement, have been formulated. The non-uniform stress distribution was analytically solved by using the complex functions. The displacement boundary condition applied to the concrete cylinder was derived as a function of the time-dependent corrosion rate. Further, the time to initiation of concrete cracking has been determined based on the model developed, given values of the key material and corrosion parameters. It has been demonstrated that the developed analytical model can simulate the stresses in concrete caused by non-uniform corrosion and predict the time to cracking initiation. The model has also been partially verified due to the limitation of available test data on non-uniform corrosion directly. The developed model can be practically used by industrial engineers and asset managers for their decision-making in regards to corrosion induced concrete cracking problems.

ACKNOWLEDGEMENT

Financial support from European Commission via the Marie Curie IRSES project GREAT under FP7-PEOPLE-2013-IRSES-612665, Scottish Funding Council GRPe for early career researcher exchanges and Australian Research Council under DP140101547, LP150100413 and DP170102211 is gratefully acknowledged.

REFERENCES

Andrade C, Alonso C and Molina FJ (1993) Cover cracking as a function of bar corrosion: part I-experimental test. *Materials and Structures* 26**:** 453-464.

Bazant ZP (1979) Physical model for steel corrosion in concrete sea structures - theory. *Journal of the Structural Division-ASCE* 105**:** 1137-1153.

Bhargava K, Ghosh AK, Mori Y and Ramanujam S (2006) Model for cover cracking due to rebar corrosion in RC structures. *Engineering Structures* 28**:** 1093-1109.

Du YX, Jin WL and Zhang R (2014) Modeling the cracking of cover concrete due to non-uniform corrosion of reinforcement. *Corrosion Science,* 89**,** 189-202.

EL Maaddawy, T, Soudki K and Topper T (2005) Analytical model to predict nonlinear flexural behavior of corroded reinforced concrete beams. *ACI Structural Journal* 102**:** 550-559.

González, JA, Andrade C, Alonso C and Feliu S (1995) Comparison of rates of general corrosion and maximum pitting penetration on concrete embedded steel reinforcement. *Cement and Concrete Research* 25**:** 257-264.

Jang, BS and Oh BH (2010) Effects of non-uniform corrosion on the cracking and service life of reinforced concrete structures. *Cement and Concrete Research* 40**:** 1441-1450.

Koch, GH, Brongers MPH, Thompson NG, Virmani YP and Payer JH (2002) Corrosion cost and preventive strategies in the United States. Federal Highway Administration, United States.

Li, CQ (2003) Life cycle modelling of corrosion affected concrete structures - propagation. *ASCE Journal of Structural Engineering* 129**:** 753-761.

Li, CQ, Melchers RE and Zheng JJ (2006) Analytical model for corrosion-induced crack width in reinforced concrete structures. *ACI Structural Journal* 103**:** 479-487.

Li CQ and Yang ST (2011) Prediction of concrete crack width under combined reinforcement corrosion and applied load. *ASCE Journal of Engineering Mechanics* 137**:** 722-731.

Liu Y and Weyers RE (1998) Modelling the time-to-corrosion cracking in chloride contaminated reinforced concrete structures. *ACI Materials Journal* 95**:** 675-681.

Mullard JA, and Stewart MG (2011) Corrosion-induced cover cracking: new test data and predictive models. *ACI Structural Journal* 108**:** 71-79.

Muskhelishvili NI (1953) *Some basic problems of the mathematical theory of elasticity,* Holland, P. Noordhoff Ltd.

Otsuki N, Miyazato S, Diola NB and Suzuki H (2000) Influences of bending crack and water-cement ratio on chloride-induced corrosion of main reinforcing bars and stirrups. *ACI Materials Journal* 97**:** 454-464.

Pan T and Lu Y (2012) Stochastic modeling of reinforced concrete cracking due to nonuniform corrosion: FEM-based cross-scale analysis. *ASCE Journal of Materials in Civil Engineering* 24(6): 698-706.

Pantazopoulou SJ and Papoulia KD (2001) Modeling cover cracking due to reinforcement corrosion in RC structures. *ASCE Journal of Engineering Mechanics* 127**:** 342-351.

Sadd MH (2005) *Elasticity: theory, application and numerics,* USA, Elsevier Butterworth-Heinemann.

Tepfers R (1979) Cracking of concrete cover along anchored deformed reinforcing bars. *Magazine of Concrete Research* 31**:** 3-12.

Yuan Y and Ji Y (2009) Modeling corroded section configuration of steel bar in concrete structure. *Construction and Building Materials* 23**:** 2461-2466.

Zhao Y, Karimi AR, Wong HS, Hu B, Buenfeld NR and Jin W (2011) Comparison of uniform and non-uniform corrosion induced damage in reinforced concrete based on a Gaussian description of the corrosion layer. *Corrosion Science* 53**:** 2803-2814.

LIST OF TABLES

Table 1 Units of the parameters

Parameter	**Unit**
D / d_0	mm
ρ_{rust} / ρ_{st}	kg / m^3
α_{rust}	n.a.
$W_{rust} / W_s / W_0 / W_m$	mg / mm
$d_m(t)$	m
i_{corr}	$\mu\ A / cm^2$
t	year

491
492 Table 2 Values of basic variables used in cracking computation
493

Symbol	Values	Sources
C	31 mm	Li (2003)
D	12 mm	Li (2003)
d_0	12.5 μm	Liu and Weyers (1998)
E_{ef}	18.82 GPa	Li (2003)
f_t	5.725 MPa	Li (2003)
i_{corr}	$0.3686ln(t)+1.1305$ μA/cm^2	Li (2003)
α_{rust}	0.57	Liu and Weyers (1998)
ν	0.18	Liu and Weyers (1998)
G	$E/[2(1+\nu)]$	Timoshenko and Goodier (1970)
ρ_{rust}	3600 kg/m^3	Liu and Weyers (1998)
ρ_{st}	7850 kg/m^3	Liu and Weyers (1998)

494
495

496 Table 3 Comparison of time to cracking initiation
497

Specimen	D (mm)	C (mm)	f_t (MPa)	E_{ef} (GPa)	Time to cracking initiation from experiments (Mullard and Stewart, 2011) (hours)	Time to cracking initiation from the model (hours)
1	16	50	2.40	18.82	35	43
2	27	50	2.40	18.82	26	59
3	16	42	3.79	18.82	45	49
4	27	36	3.79	18.82	43	68

498

LIST OF FIGURES

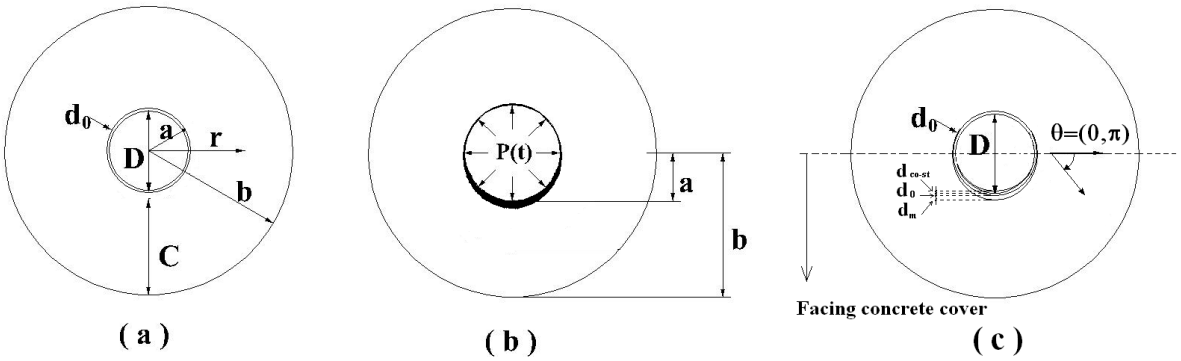

516

517 Figure 1 Illustration of non-uniform internal pressure caused by reinforcement corrosion

518

519

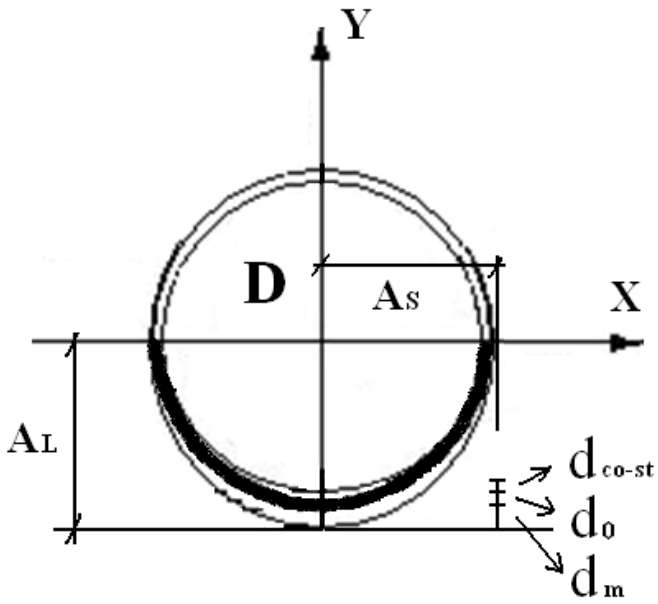

520
521 Figure 2 Schematic of the bands filled by corrosion products
522

523

524

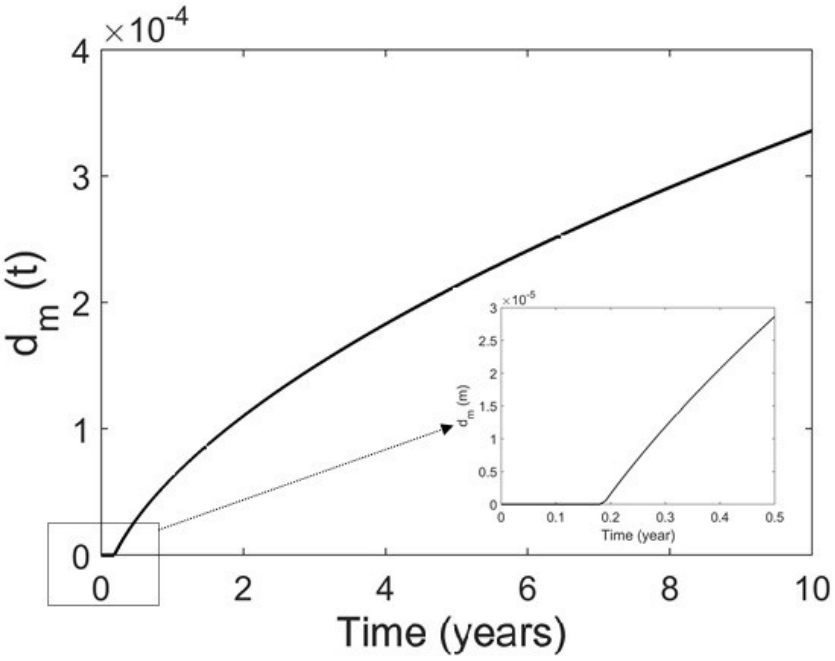

Figure 3 $d_m(t)$ as a function of service time

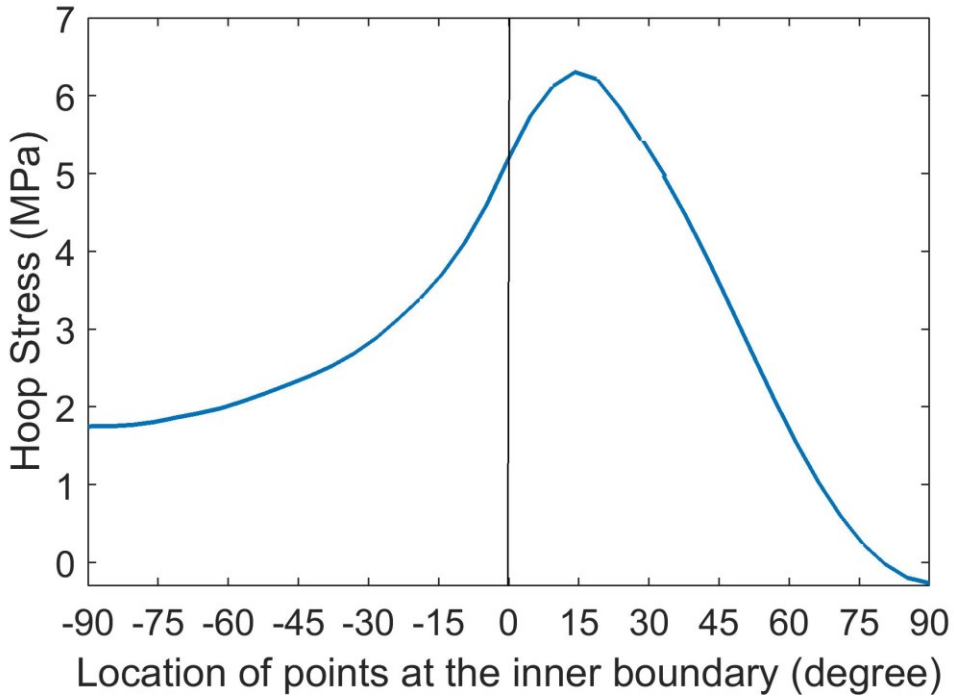

531

532 Figure 4 Hoop stress distribution at the inner boundary of the concrete at the time of 0.23 year

533

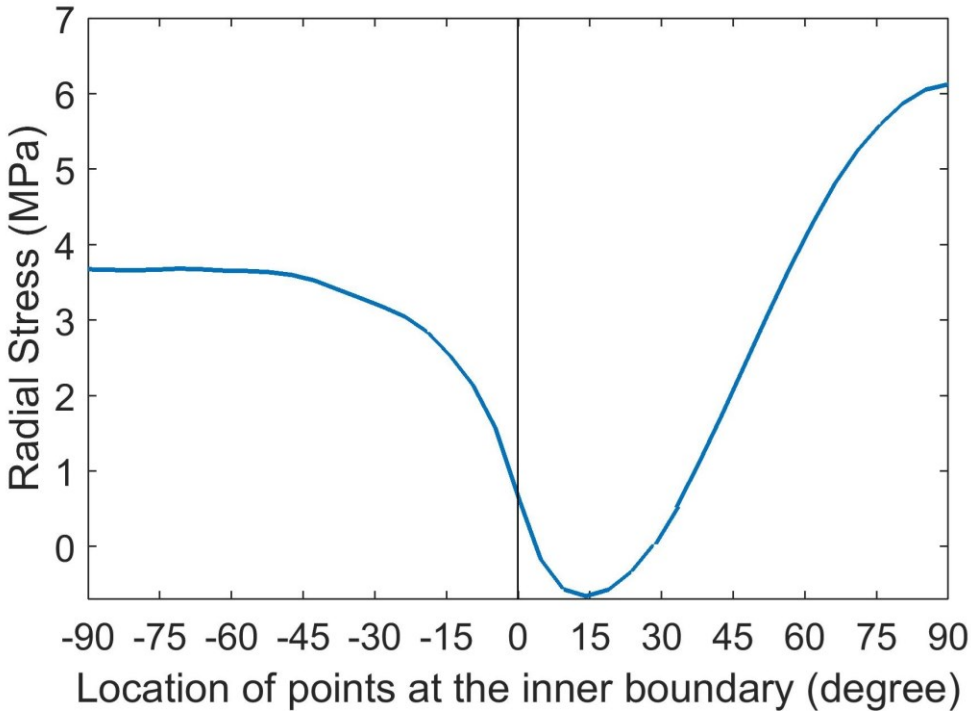

534

535 Figure 5 Radial stress distribution at the inner boundary of the concrete at the time of 0.23 year

536

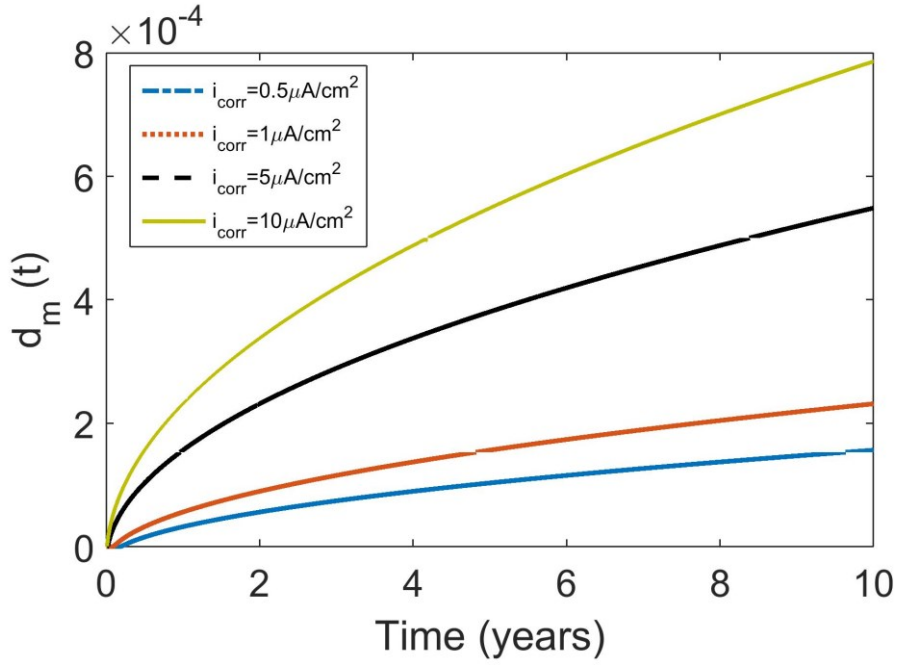

537

538 (a)

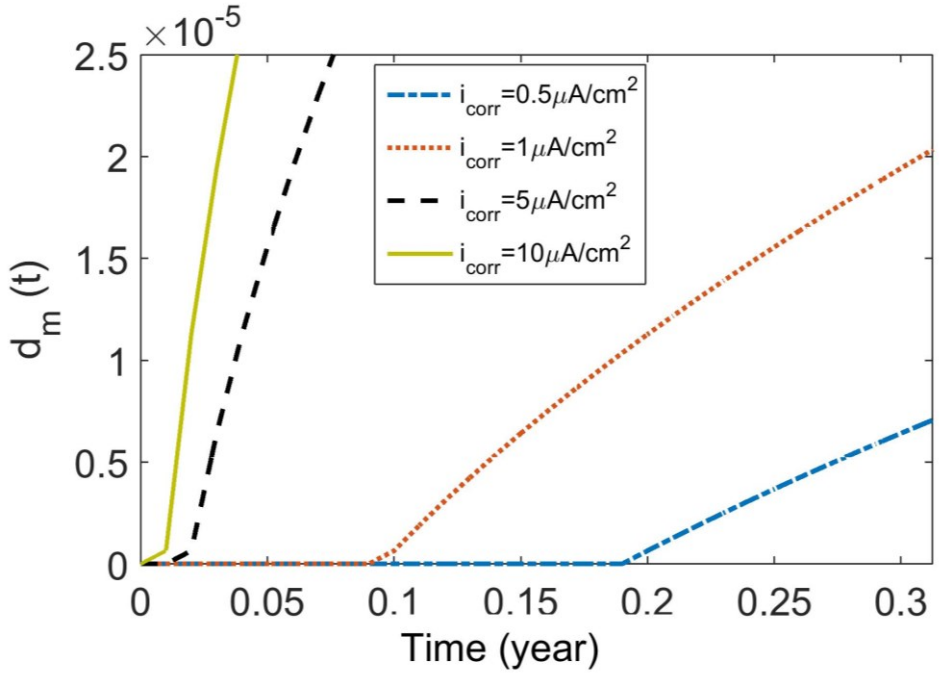

539

540 (b)

541 Figure 6 (a) Effects of the corrosion rate i_{corr} on the development of displacement $d_m(t)$ as a

542 function of service time; (b) enlarged view of $d_m(t)$ at the initial period

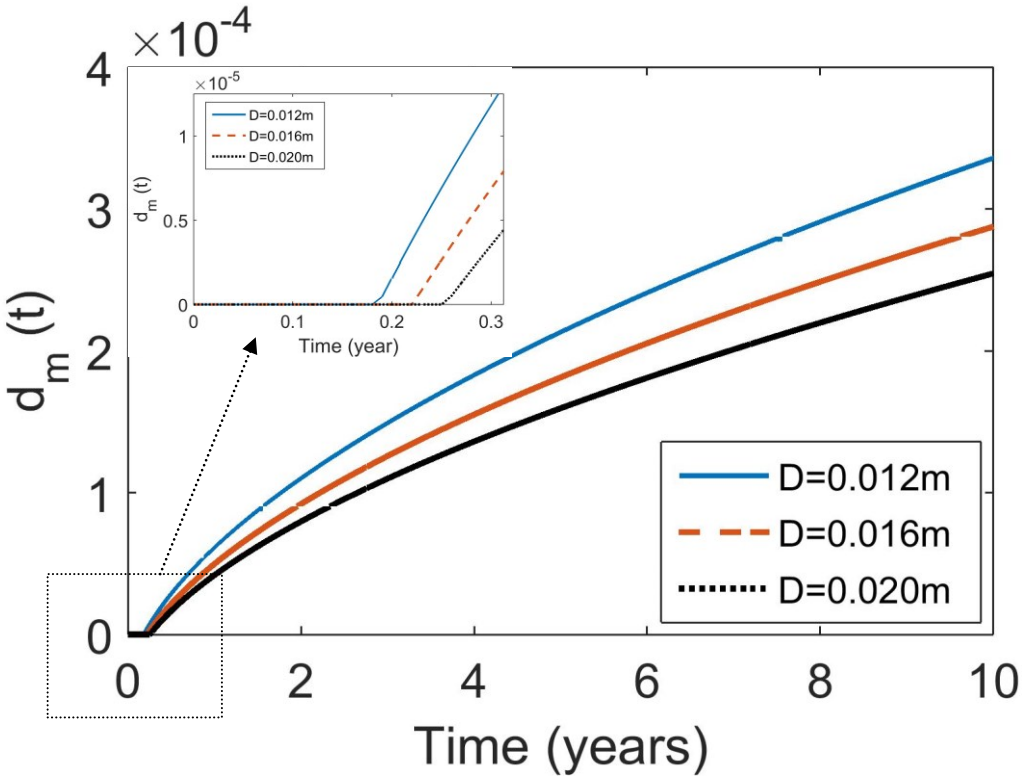

Figure 7 Effects of the diameter of the rebar D on the progression of $d_m(t)$

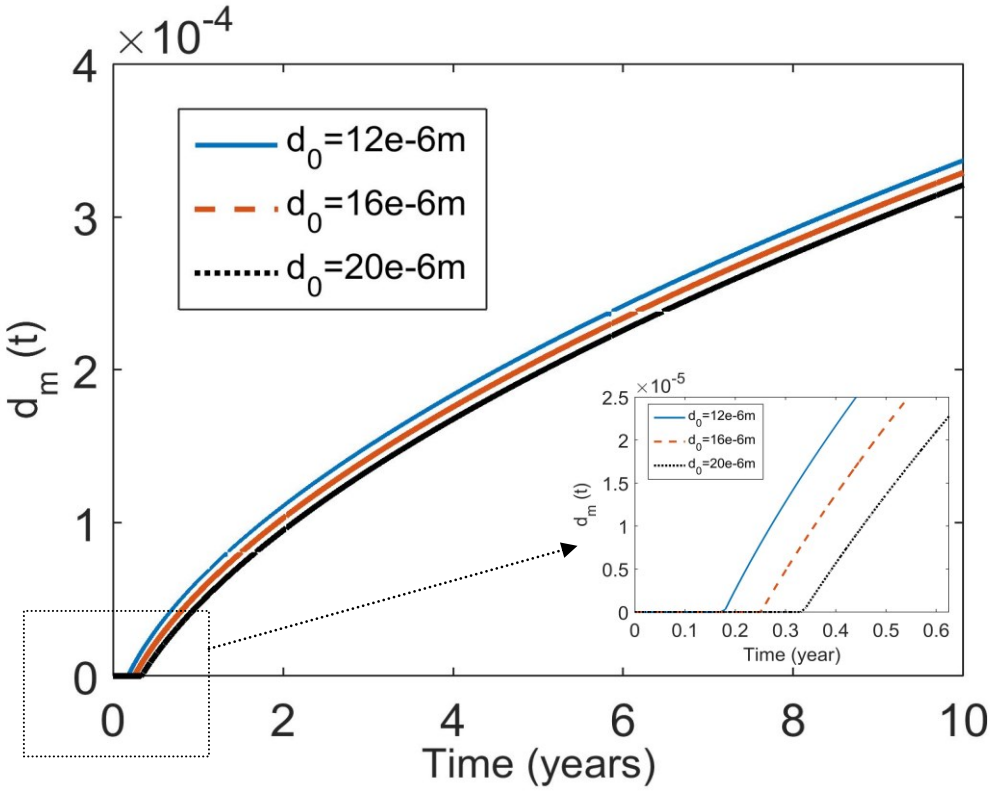

Figure 8 Effects of the thickness of the ITZ on the progression of $d_m(t)$

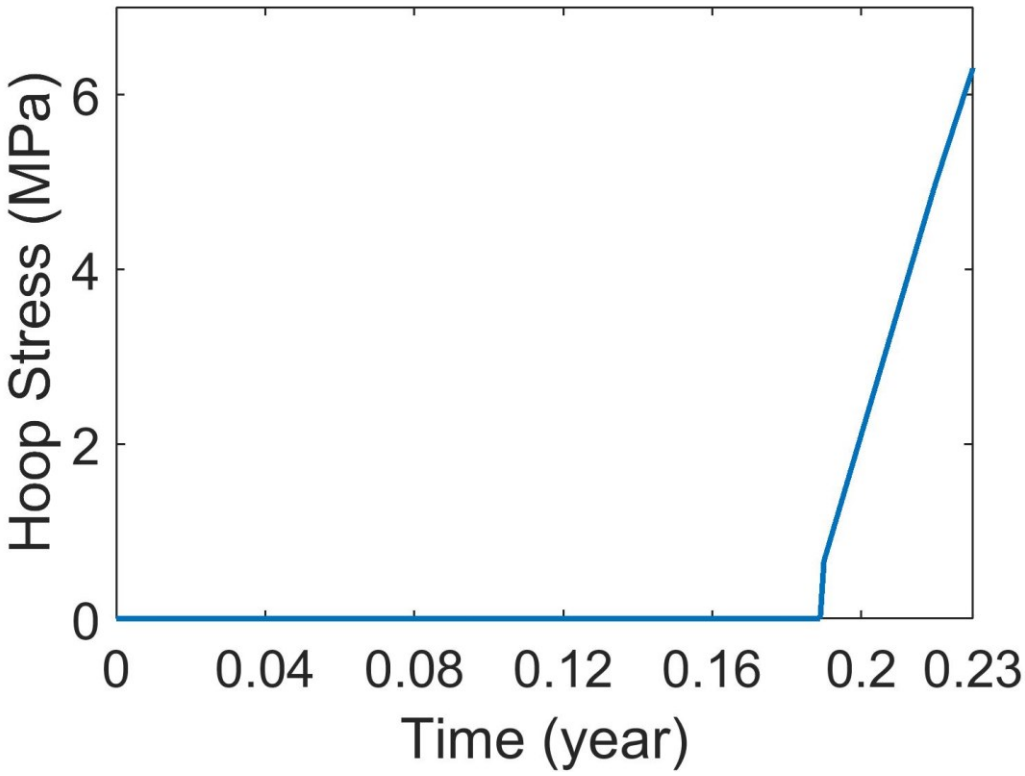

Figure 9 Hoop stress development as a result of the non-uniform corrosion process for the location of 15^0

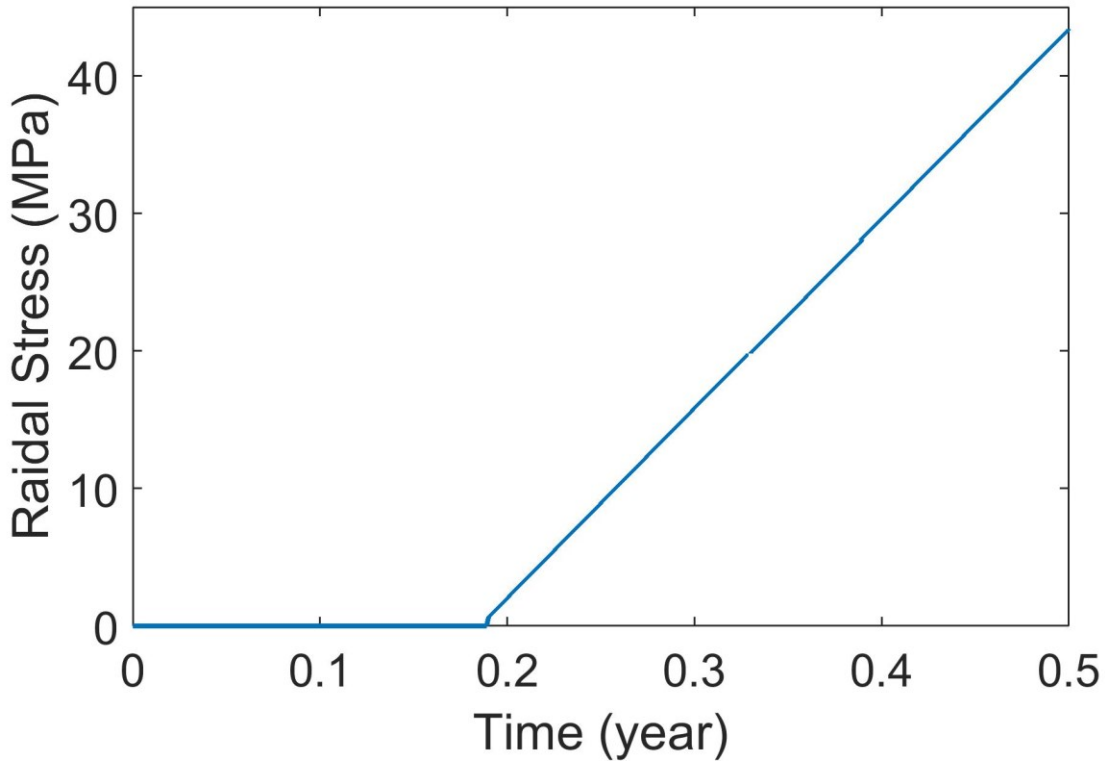

571

572 Figure 10 Radial stress development as a result of the non-uniform corrosion process for the

573 location of 90^0

574

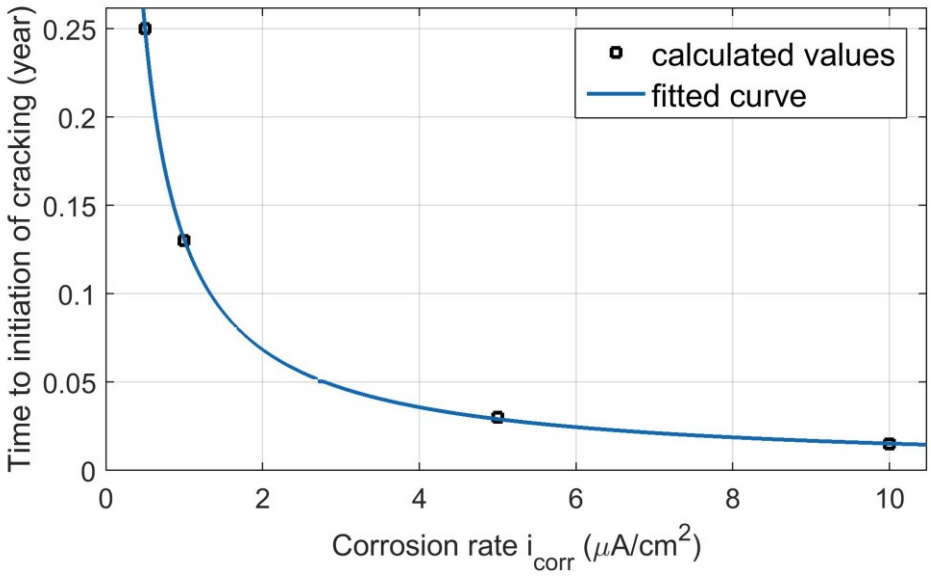

575

576 Figure 11 Time to the initiation of concrete cracking as a function of the corrosion rate

577

578